

# Identity fast ion phase space loss region in W7-X Stellarator

Qien Jing<sup>1</sup>, Ethan Green<sup>2</sup>, Xishuo Wei<sup>2</sup>, Huishan Cai<sup>3</sup>, Zhihong Lin<sup>2</sup>

<sup>1</sup>University of Science and Technology of China, Hefei 230026, China

<sup>2</sup>CAS Key Laboratory of Frontier in Controlled Nuclear Fusion, and School of Nuclear Sciences and Technology, University of Science and Technology of China

<sup>3</sup>Department of Physics and Astronomy, University of California, Irvine, CA 92697, United States of America

E-mail: [hscai@mail.ustc.edu.cn](mailto:hscai@mail.ustc.edu.cn)

November 2024

**Abstract.** Based on the Gyrokinetic Toroidal Code (GTC), the lost particles structure in fast ion phase space, lost mechanism and radial electric field ( $E_r$ ) on lost particles in W7-X stellarator are investigated. The lost particles structure is mainly in the area of minimum magnetic field contours region and the magnetic field contours symmetrically beside this region. The dominant lost particle category is deeply helical-trapped particle. Using constant  $E_r$  as an approximation, the results show that each sign of the constant  $E_r$  improves the particles confinement, and the dominant lost particle category does not change. Because of the additional rotation induced by  $E_r$ , the ion root  $E_r$  cause the deeply helical-trapped lost particles structure locate near the out midplane, and the deeply helical-trapped particles initially from minimum  $|B|$  contours region gain good confinement. The electron root  $E_r$  causes the deeply helical-trapped particles to become the only lost particles category, and the loss is mostly due to the fast outward drift when particles cross the out midplane.

Keywords: stellarator, W7X, lost particle

## 1. Introduction

The Wendelstein 7-X (W7-X) is a stellarator to approach quasi-isodynamicity (QI) [1], which was optimized for good MHD stability, good finite beta equilibrium properties, improved neoclassical confinement, good collisionless  $\alpha$  particle containment, and low bootstrap currents [2, 3]. It is designed to use an NBI system has the capacity to be equipped with D<sup>0</sup> (60kV) and H<sup>0</sup> (55kV) source [4].

Previous studies have shown that the L-H transition[5] is related to the radial electric field  $E_r$ , and the  $E_r$  shear has a stabilizing effect on microturbulence and reduces the turbulent transport level to improve the plasma confinement [6, 7, 8, 9]. Therefore, the formation of  $E_r$  has been widely studied. The various factors influencing  $E_r$  formation and the relationships between them are thoroughly discussed in [10]. The

profile of  $E_r$  can be determined by the toroidal and poloidal plasma rotation and ion pressure gradient. The neutral beam injection (NBI) can generate  $E_r$  by enhancing the plasma rotation in toroidal and poloidal direction, which does not depend on  $E_r$ . Additionally,  $E_r$  can be created by non-ambipolar flux, because NBI can produce fast ion by charge exchange and ionization process, the loss of these fast ion will cause effective ion flux. Therefore, it is important to study the dominant lost region in phase space in order to create fast ion flux and manipulate  $E_r$  [10]. Previous studies on W7-X have discussed about NBI ion wall loads in various plasma scenarios [11]. The research on neoclassical ambipolar electric field [12] indicate the electric field magnitude is on the order of  $10^4$  kV/m for both ion and electron roots. Moreover, the fast ion lost channel as well as the influence of  $E_r$  on the lost channel are studied in [13]. Meanwhile, there is still a few research on the analysis of lost particles structure in phase space and the impact of  $E_r$  on the dominant lost regions in phase space.

In this work, using Gyrokinetic Toroidal Code (GTC), the lost particles structure in fast ion phase space and the lost mechanism in W7-X stellarator are investigated. We found that the  $\Delta N/N$  as a function of the particles initial positions in  $\theta - \zeta$  plane is mainly in the minimum  $|B|$  contours region and the magnetic field contours symmetrically beside the minimum  $|B|$  contours region. The deeply helical-particles with the largest  $\lambda$  is the dominant loss channel. For lost particles from the flux surface near magnetic axis, a  $\lambda$  gap for the lost particles in the  $E - \lambda$  phase space was found, which gradually disappears with increasing  $\psi/\psi_w$  because the magnetic contour is rougher and deviates further from the ideal QI configuration. Besides, using constant radial electric field ( $E_r$ ) as an approximation, the effect of  $E_r$  on lost particles in W7-X stellarator is studied. The result shows that each sign of the constant  $E_r$  improves the particles confinement and the reduction of  $\Delta N/N$  is proportional to the  $E_r$  magnitudes. Because of the additional poloidal rotation, under the electron root and ion root  $E_r$ , toroidally trapped particles still has very good confinement properties and barely helical-trapped particles achieves better confinement. Under ion root  $E_r$ , the barely helical-trapped particles gain better confinement due to the additional rotation. The deeply helical-particles that be lost are not initially located in the minimum  $|B|$  contours as the No  $E_r$  result, but are located near the out midplane. Under electron root  $E_r$ , the barely helical-trapped particles are almost completely confined because of the additional rotation, and the deeply helical-trapped particles are the only type of lost particles. The trapped particles are likely to lose confinement when crossing the out midplane, then be trapped near the flux surface near the edge and lost due to the larger orbit width.

The remainder of this paper is organized as follows. The physical model and simulation setup are described in section 2. The lost structure in fast ion phase space and lost mechanism is discussed in section 3. The effect of  $E_r$  on lost particles is discussed in section 4. Section 5 gives a summary of the study.

## 2. Simulation model and setup

In this work, fast ion guiding center trajectories in the W7-X are calculated by the GTC using the drift kinetic equation for the distribution function  $f$  in the collisionless limit,

$$\frac{d}{dt} f(\mathbf{X}, \mu, v_{\parallel}, t) \equiv \left[ \frac{\partial}{\partial t} + \dot{\mathbf{X}} \cdot \nabla + \dot{v}_{\parallel} \frac{\partial}{\partial v_{\parallel}} \right] f = 0 \quad (1)$$

where  $\mathbf{X}, \mu, v_{\parallel}$  are the guiding center position, magnetic moment, and parallel velocity respectively. We can write  $\dot{\mathbf{X}}$  and  $v_{\parallel}$  as

$$\dot{\mathbf{X}} = v_{\parallel} \mathbf{b}_0 + \mathbf{v}_E + \mathbf{v}_d \quad (2)$$

$$\dot{v}_{\parallel} = -\frac{1}{m} \frac{\mathbf{B}^*}{B_0} \cdot (\mu \nabla B_0 + Z \nabla \phi) \quad (3)$$

where  $Z$  is the ion charge,  $m$  is the ion mass,  $\mathbf{B}_0 = B_0 \mathbf{b}_0$  is the equilibrium magnetic field,  $\mathbf{b}_0 = \mathbf{B}/B_0$  is the unit vector of magnetic field,  $\mathbf{b}^* = \mathbf{b}_0 + \frac{v_{\parallel}}{\Omega} \nabla \times \mathbf{b}_0$  is the modified magnetic field unit vector,  $\Omega = \frac{ZB_0}{mc}$  is the cyclotron frequency,  $\mathbf{v}_E = \frac{c\mathbf{b}_0 \times \nabla \phi}{B_0}$  is the drift velocity of the electric field,  $\mathbf{v}_d = \frac{\mu}{m\Omega} \mathbf{b}_0 \times \nabla B_0 + \frac{v_{\parallel}^2}{\Omega} \nabla \times \mathbf{b}_0$  is the magnetic drift velocity. To account for the influence of the ambipolar radial electric field  $E_r$ , a model electrostatic potential  $\phi$  is included in the simulation.

A model W7-X stellarator geometry is used in this work [14]. The 3D equilibrium is described by using Boozer coordinates  $(\psi, \theta, \zeta)$ , where  $\psi$  is poloidal flux,  $\theta$  is poloidal angle, and  $\zeta$  is toroidal angle [15]. Our simulation domain is in the normalized flux function  $\psi/\psi_w = [0.01, 1.00]$  ( $\psi$  is the poloidal magnetic flux and  $\psi_w$  the magnetic flux at the wall) and one-fifth of the W7-X torus is used because of the toroidal periodicity. To study the loss region in the fast ion phase space, we uniformly load the fast ion in 5D phase spaces  $(\psi, \theta, \zeta, v_{\parallel}, E)$  to sample the phase space efficiently. It is convenient to use the conserved quantities energy  $E$  and pitch angle  $\lambda = \mu B_0/E$  to identify the lost particles in phase space, where  $B_0$  is the magnetic field amplitude at the magnetic axis at  $\zeta = 0$  with the stellarator up-down symmetry. Consider the maximum particle energy of NBI system in the W7-X is 55 keV [4], the particle energy is uniformly loaded in the range of  $E = [0, 55]$  keV. The first orbit lost particles are excluded in the following results, as the NBI fast ions are not injected near the plasma edge. The time step of the orbit integration is  $\Delta t = 0.01 R_0/C_s$ , where  $R_0$  is the major radius at  $\zeta = 0$  and  $C_s = \sqrt{kT_e/m_i}$  is the sound speed on the magnetic axis, with  $k$  being the Boltzmann constant,  $T_e$  the electron temperature on the magnetic axis, and  $m_i$  the ion mass.

## 3. Identification of lost particles in phase space without $E_r$

### 3.1. Orbit analysis of lost particles

The analysis of lost particles focuses on the trapped particles, as passing particles typically exhibit good confinement. The trapped particle orbits in W7-X can be divided

into two main categories: helically trapped particles, whose orbits are constrained to the local minimal magnetic field region within a single toroidal period due to the mirror  $B(m = 0, n = 5)$  and helical  $B(m = 1, n = 5)$  variations of the  $B$  field, and the toroidally trapped particles, whose orbits are not constrained by the global maximal magnetic field due to the toroidal  $B(m = 1, n = 0)$  variations of the  $B$  field. The representative guiding center orbits are compared in figure 1. Besides the guiding center trajectories (blue line), the black dashed line in the upper panel show the contours of the magnetic field amplitude  $|B|$  and the lower panel the flux surfaces at  $\psi/\psi_w = 0.2, 0.4, 0.6, 0.8, 1.0$ . The orbit shown in figure. 1a is toroidally trapped particles, and those in figure. 1b and figure. 1c are the barely and deeply helically trapped particle, respectively. The toroidally and helically trapped particles were fully discussed in [13]. The barely helically trapped particles have different characteristics compared to the other two types. Take particle orbit in figure. 1b as an example, the barely helically trapped particles are confined within a single toroidal period, behaving similarly to the deeply helically trapped particles shown in figure. 1c. However, they exhibit longer toroidal motion compared to deeply helically trapped particles, allowing them to reach a higher magnetic wall. Moreover, the barely helically trapped particles demonstrate a greater tendency to be lost, in contrast to the good confinement of toroidally trapped particles.

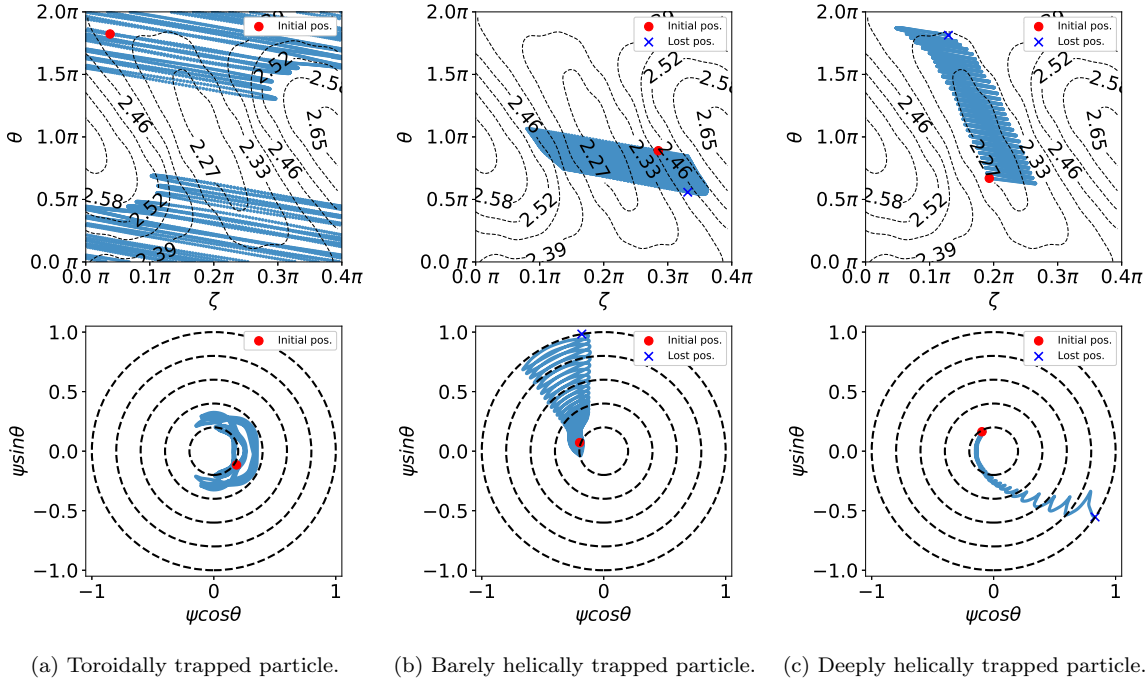


Figure 1: The guiding center orbits of (a) a toroidally trapped particle with  $\lambda = 0.945$  and  $E = 45.6$  keV, (b) a barely helically trapped particle, lost at  $53.82 C_s/R_0$ , with  $\lambda = 0.964$  and  $E = 47.7$  keV, and (c) a deeply helically trapped particle, lost at  $36.67 C_s/R_0$ , with  $\lambda = 1.051$  and  $E = 53.2$  keV on a flux surface (upper panels) and on a poloidal plane (lower panels).

### 3.2. Loss regions in the fast ion phase space

The  $(\Delta N/N)$  is defined to represent the proportion of total lost particles relative to the total number of particles, where  $N$  is the total particles number and  $\Delta N$  is the lost particle number excluding the first orbit lost particles. The cumulative  $\Delta N/N$  increases as time passes, as shown in figure. 2a. The  $\Delta N/N$  at  $t = 120 R_0/C_s$  as a function of particles initial radial position at  $t = 0 R_0/C_s$  is shown in the figure figure. 2b. The dominant initial radial position of lost particles is around  $\psi/\psi_w = 0.85$  (normalized minor radius  $r/a = 0.92$ ), which is near the last closed flux surface. Nonetheless, there is still half of the highest  $\Delta N/N$  at the  $\psi/\psi_w = 0.50$  ( $r/a = 0.72$ ) flux surface, which is caused by the radial drift of trapped particles. The  $\Delta N/N$  as a function of particles initial positions in both the  $\theta - \zeta$  plane and the  $E - \lambda$  phase space are shown in the figure. 3. It can be seen that the loss region mainly locates in the minimum  $|B|$  region and extends along the magnetic field line in the  $\theta - \zeta$  plane. The  $\Delta N/N$  in the  $E - \lambda$  phase space (figure. 3b) shows a major loss region  $\lambda \geq 1.04$ , and a secondary loss region  $0.80 \leq \lambda \leq 1.04$ . Virtually no losses are observed for  $\lambda \leq 0.08$ . Additionally, for a fixed  $\lambda$ , the  $\Delta N/N$  decrease with decreasing energy , which indicates that particles with higher energy are more likely to be lost. Furthermore, the two loss regions in the  $E - \lambda$  phase space (i.e.,  $0.80 \leq \lambda \leq 1.04$  and  $\lambda \geq 1.04$ ) correspond to two loss regions in the  $\theta - \zeta$  space shown in figure. 4a and figure. 4b, respectively. So, the two loss regions in the  $E - \lambda$  phase space are also separated in real space. The dominant lost particles with  $\lambda \geq 1.04$  are deeply helically trapped particles initially located in the region of the minimum  $|B|$  region in the  $\theta - \zeta$  space. While the initial position of the secondary lost particles with  $0.80 \leq \lambda \leq 1.04$  are mostly barely helically trapped particles initially located in the  $\theta - \zeta$  space with  $B < 2.68$  T.

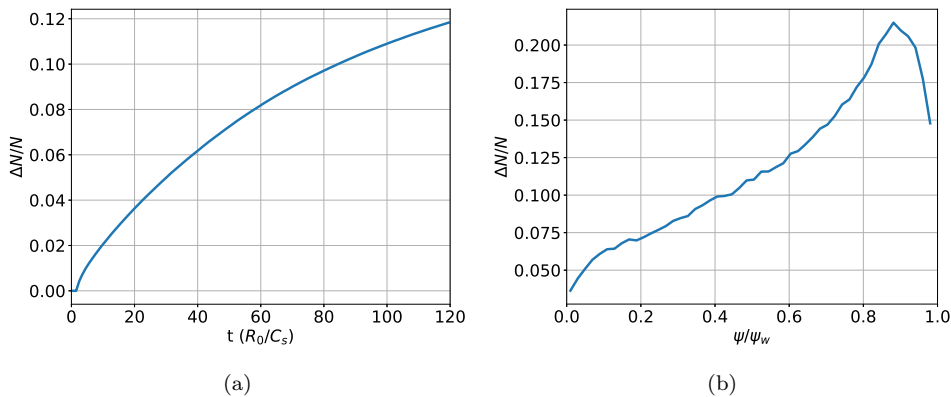


Figure 2: (a) Cumulative  $\Delta N/N$  during the simulation for  $t = [0, 120] R_0/C_s$ . (b) The  $\Delta N/N$  at  $t = 120 R_0/C_s$  as a function of particles initial radial position at  $t = 0 R_0/C_s$ .

Next, the  $\Delta N/N$  as a function of particles initial positions in the  $\theta - \zeta$  space and the  $E - \lambda$  phase space at different initial radial positions is shown in figure. 5. Four different radial regions are considered  $\psi/\psi_w = [0.18, 0.22], [0.38, 0.42], [0.58, 0.62], [0.78, 0.82]$ , corresponding to the representative flux surfaces at  $\psi/\psi_w = 0.2, 0.4, 0.6, 0.8$ . At the

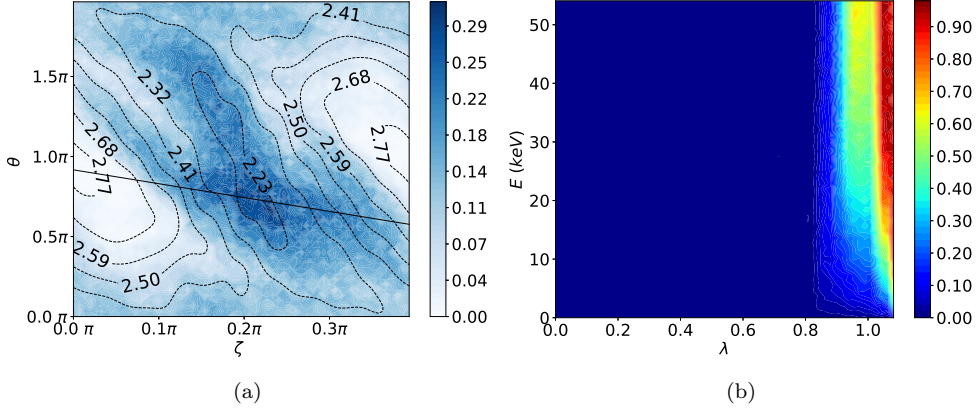


Figure 3: The  $\Delta N/N$  as a function of particles initial positions in the  $\theta - \zeta$  plane (panel a) and the  $E - \lambda$  phase space (panel b). The dashed contours represents the magnetic field amplitude (T), and the solid line indicates a magnetic field line at the flux surface  $\psi/\psi_w = 0.8$ .

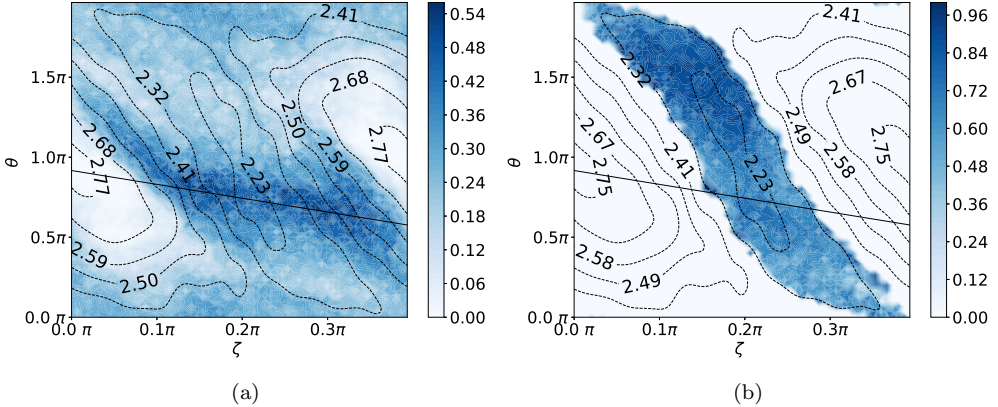


Figure 4: The  $\Delta N/N$  as a function of particles initial positions in the  $\theta - \zeta$  plane for the ranges  $0.80 \leq \lambda \leq 1.04$  (Panel a) and  $1.04 \leq \lambda$  (Panel b).

innermost flux surface  $\psi/\psi_w = 0.2$ , the loss regions are clearly separated in the  $\theta - \zeta$  space and the  $E - \lambda$  phase space, while the loss regions gradually mixed together in the  $\theta - \zeta$  space and the  $E - \lambda$  phase space with increasing  $\psi/\psi_w$ . The variation in the contours of  $B$  accounts for this observation. As  $\psi/\psi_w$  increases, the initially smooth contours gradually become wavy, and the contours line on the left, central, and right regions progressively merge, resulting in the gradual disappearance of the previously observed gap.

Finally, we focus on the specific radial position  $\psi/\psi_w = 0.20$ , because it is close to the magnetic axis and can serve as an effective position for manipulating  $E_r$  by NBI to improve the particle confinement. Based on the separated loss regions in the  $E - \lambda$  phase space shown in figure 5e, the  $\Delta N/N$  as a function of particles initial positions in the  $\theta - \zeta$  plane can be categorized into three distinct patterns based on different  $\lambda$  values. The  $\Delta N/N$  as a function of particles initial positions with different  $\lambda$  values in the  $\theta - \zeta$  plane at the flux surface  $\psi/\psi_w = 0.20$  is shown in figure 6. The lost particles with  $\lambda = [0.9, 1.0]$  are mostly located near the contours of  $B = 2.52$  T. There fewer

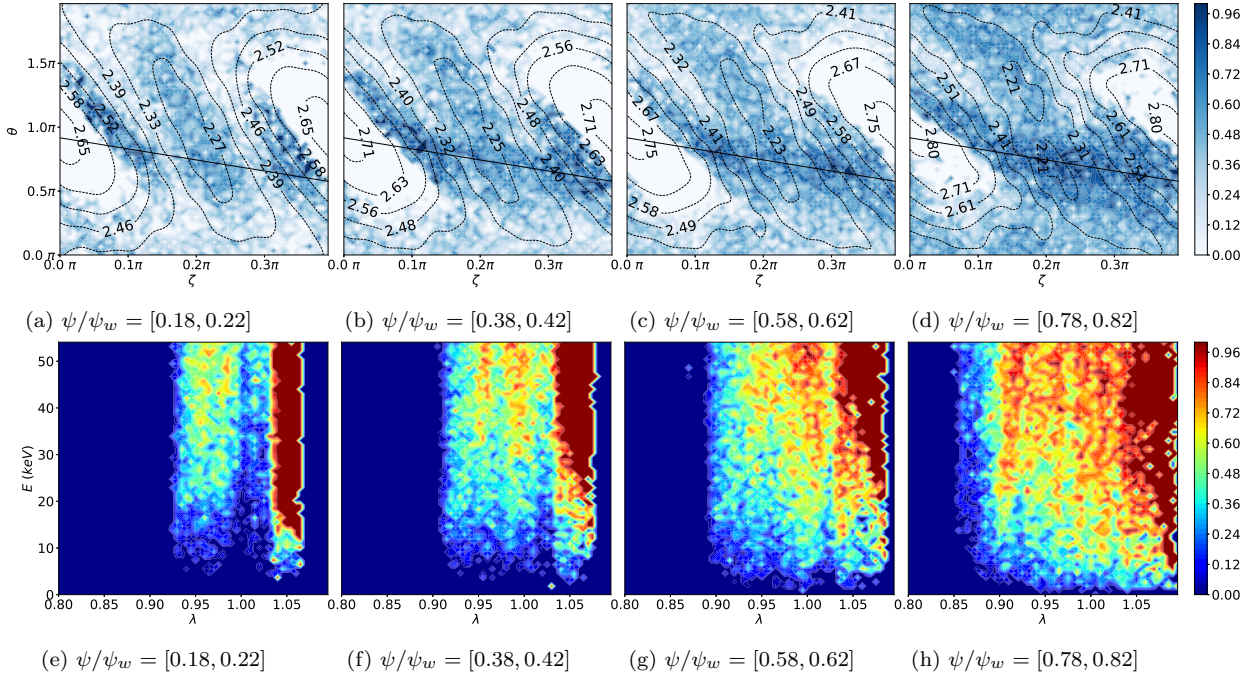


Figure 5: (a)-(d) The  $\Delta N/N$  as a function of particles initial positions in the  $\theta - \zeta$  plane at  $\psi/\psi_w = 0.2, 0.4, 0.6, 0.8$ . (e)-(h) The  $\Delta N/N$  in the  $E - \lambda$  phase space at  $\psi/\psi_w = 0.2, 0.4, 0.6, 0.8$ . Noticed that the black solid line in upper row is same as the one in figure. 3a, because of the safety factor  $q$  in W7-X is nearly constant, and the dash line represent the contours of  $|B|$ .

lost particles with  $\lambda = [1.000, 1.035]$  than lost particles with other  $\lambda$  values, and these particles are initially located in the region that has medium  $B$  values. The lost particles with  $\lambda = [1.035, 1.100]$  are initially located in the lowest  $B$  region and have the highest  $\Delta N/N$  compared to the lost particles with other  $\lambda$  values. In summary, in the specific radial position  $\psi/\psi_w = 0.2$ , the particles initially located in the lowest  $B$  region with  $\lambda > 1.035, E > 20$  keV are most likely to be lost.

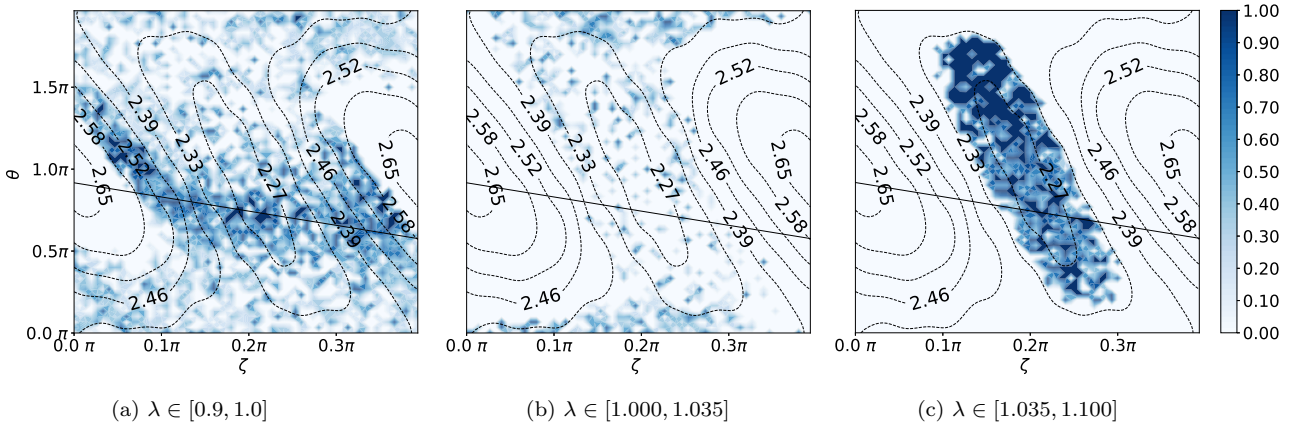


Figure 6: The  $\Delta N/N$  as a function of particles initial positions in the  $\theta - \zeta$  plane of three different  $\lambda$  values at the flux surface  $\psi/\psi_w = 0.20$ . Noticed that the black solid line in the upper row is same as the one in figure. 3a.

#### 4. Effect of radial electric field ( $E_r$ ) on particle loss

In this section, the mechanism of reduction of particle loss caused by  $E_r$  are further investigated. In [7], the self-consistently generated neoclassical ambipolar electric field in W7-X was calculated, showing that the  $E_r$  has an amplitude on the order of  $-5 \text{ kV/m}$  and  $+10 \text{ kV/m}$ , respectively, in ion root and electron root. The study of  $E_r$  effect in this section is based on these two values. The cumulative  $\Delta N/N$  under the different  $E_r$  values is shown in figure. 7. It is interesting that both positive and negative  $E_r$  values can improve the particles confinement and the reduction of  $\Delta N/N$  is proportional to the  $E_r$  magnitudes, but independent of  $E_r$  direction. The following subsections provide a detailed analysis of the  $E_r$  effect on the guiding center orbits.

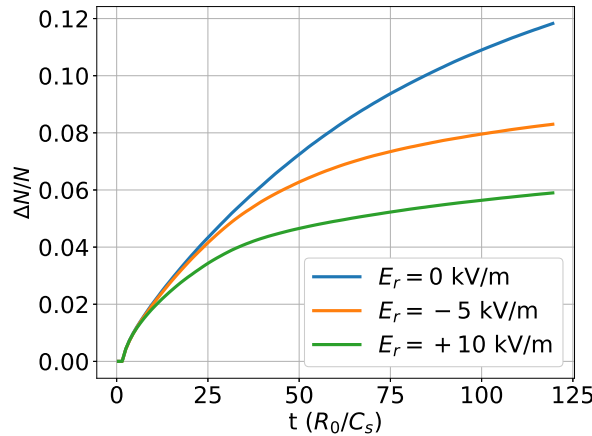


Figure 7: The cumulative  $\Delta N/N$  during the simulation for  $t = [0, 120]$   $R_0/C_s$  under the different constant  $E_r$ .

##### 4.1. Effect of $E_r$ on loss region in the fast ion phase space

The  $\Delta N/N$  as a function of particles initial positions in the  $\theta - \zeta$  plane the  $E - \lambda$  phase space at the radial positions  $\psi/\psi_w = 0.20$  under  $E_r = -5 \text{ kV/m}$  and  $E_r = +10 \text{ kV/m}$  are shown in figure. 8b, 8c, 8e, 8f, respectively, , while the reference case without  $E_r$  is presented in figure. 8a, 8d. For  $E_r = -5 \text{ kV/m}$ , the  $\Delta N/N$  as a function of particles initial positions in the  $\theta - \zeta$  plane is predominantly concentrated near  $\theta \approx 0$  and  $\theta \approx 2\pi$ , corresponding to the outer midplane. The loss region is clearly divided into two regions of  $\lambda = [0.9, 1.0]$  and  $\lambda = [1.0, 1.1]$ , which is shown in figure. 8e. So, the  $\Delta N/N$  with  $\lambda = [0.9, 1.0]$ and  $\lambda = [1.0, 1.1]$  in the  $E - \lambda$  phase space correspond to the different loss regions in the  $\theta - \zeta$  space as well, which is shown in figure. 9a, 9b. Notably, most of the lost particles with  $\lambda = [0.9, 1.0]$  are initially located in the region with the minimum  $|B|$  and along the magnetic field line in the  $\theta - \zeta$  space, which is shown in figure. 9a. This result is consistent with the  $E_r = 0$  case, as seen in the comparison between figure. 6a, 9a. For  $E_r = +10 \text{ kV/m}$ , the  $\Delta N/N$  as a function of particles initial positions in the  $\theta - \zeta$  plane is entirely in the closed contours of the minimum  $|B|$ . These

particles are the deeply helically trapped particles with  $\lambda > 1.035$  and initially located in the closed contours of the minimum  $|B|$ , shown in figure. 8c, 8f. For both positive and negative  $E_r$ , the  $\Delta N/N$  in the  $E - \lambda$  phase space is lower than in the  $E_r = 0$  case for each  $\lambda$  and energy. Moreover, in contrast to the  $E_r = 0$  case, where the  $\Delta N/N$  remains nearly constant with decreasing energy, both positive and negative  $E_r$  exhibit a decreasing  $\Delta N/N$  with decreasing energy. This indicates that fewer low energy particles are lost when  $E_r$  is present, further demonstrating its confinement enhancing effect.

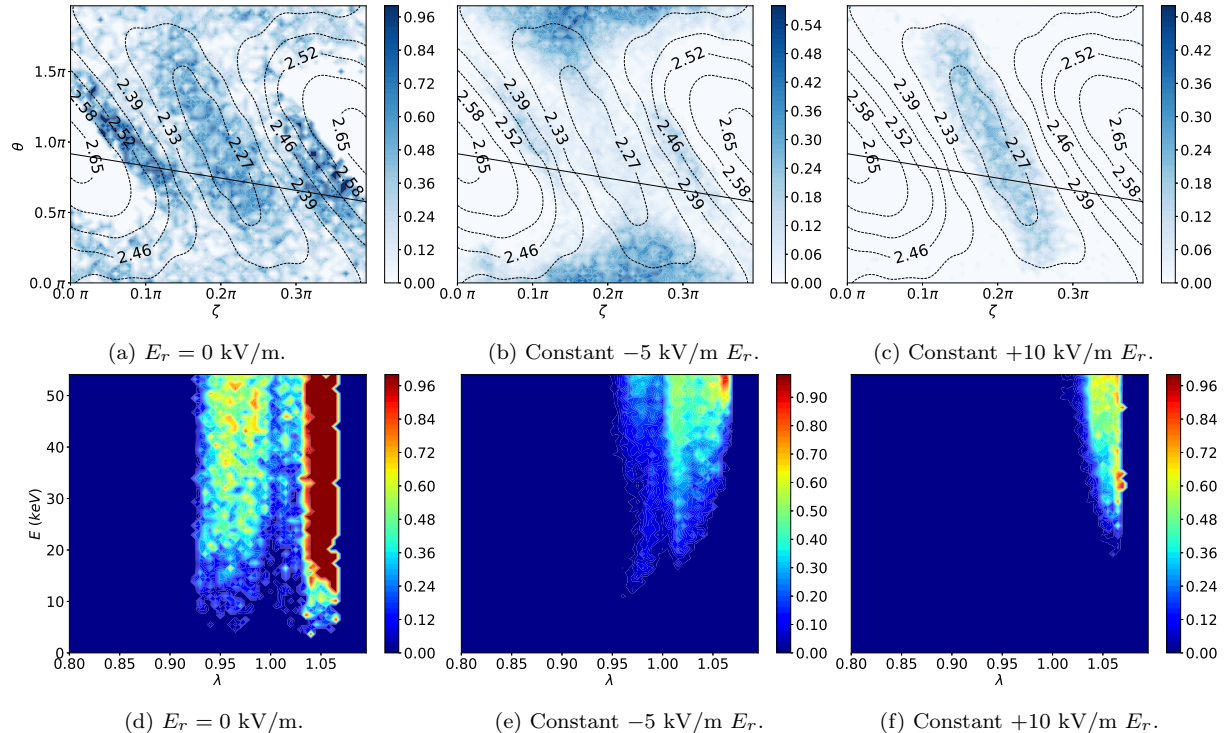


Figure 8: The  $\Delta N/N$  as a function of particles initial positions in the  $\theta - \zeta$  plane and the  $E - \lambda$  phase space at flux surfaces  $\psi/\psi_w = 0.2$  under  $E_r = 0$ ,  $E_r = -5$  kV/m and  $E_r = +10$  kV/m, respectively. The black solid line in upper row is same as the one in figure. 3a, and the dash line represent the contours of the magnetic field amplitude.

#### 4.2. Effect of $E_r$ on lost particle orbits

Due to the additional poloidal drift induced by  $E_r$ , the toroidally trapped particles maintain excellent confinement properties. The barely helically trapped particles demonstrate even more improvement of confinement under  $E_r = -5$  kV/m and  $E_r = +10$  kV/m, is shown in, respectively. The typical orbit of the barely helically trapped particle under  $E_r = -5$  kV/m and  $E_r = +10$  kV/m is shown in figure. 10a, 10b, respectively. The particles exhibit poloidal drift with  $\dot{\theta} < 0$  under  $E_r = -5$  kV/m, and  $\dot{\theta} > 0$  under  $E_r = +10$  kV/m. This directional drift enables them to avoid loss by transitioning particle orbit from barely helically trapped to toroidally trapped states. The enhanced confinement can be attributed to the fact that the inherent poloidal drift

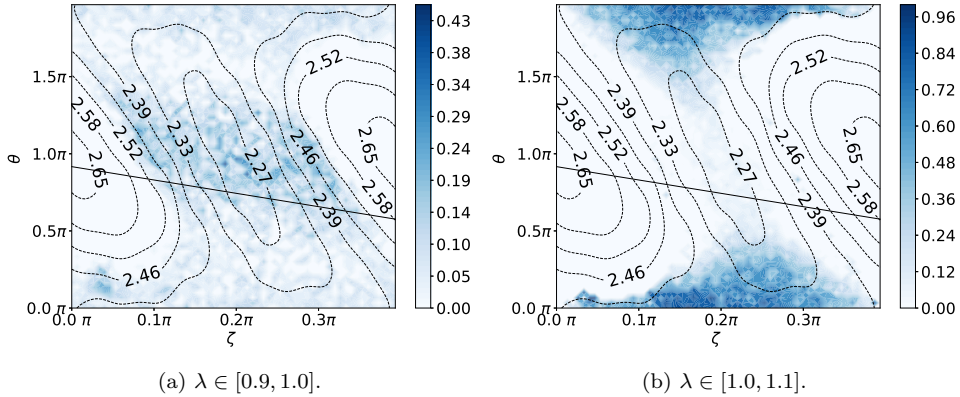


Figure 9: The  $\Delta N/N$  as a function of particles initial positions in the  $\theta - \zeta$  plane under  $E_r = -5$  kV/m with  $\lambda = [0.9, 1.0]$  (panel a) and  $\lambda = [1.0, 1.1]$  (panel b).

velocity of these particles at the red points in figure. 10a, 10b is significantly smaller than the poloidal drift velocity induced by  $E_r = -5$  kVm and  $E_r = +10$  kVm.

Next, we focus on the  $E_r$  effect on lost particle orbits. Under  $E_r = -5$  kVm, most of the deeply helically trapped particles, that initially located near  $\theta \approx 0$  and  $\theta \approx 2\pi$  region (i.e., the out midplane), experience outward drift and are rapidly lost, as exemplified in figure. 10c. The poloidal movement of these particles is negligible due to the opposing contributions from magnetic drift and  $E_r$  induced poloidal drift that nearly cancel each other. Additionally, the  $E_r$  toward the magnetic axis causes fast ion to gain potential energy during outward drift, resulting in decreased kinetic energy. The deeply helically trapped particles initially located in the closed contours of the minimum  $|B|$ , is discussed in next paragraph.

To compare the effects of different  $E_r$  profiles on the orbit of the same deeply helically trapped particle, which initially located in the contours of the minimum  $|B|$ , is shown in figure. 11a–11c. Under  $E_r = -5$  kV/m, the additional poloidal drift velocity induced by  $E_r$  partially cancels out the inherent poloidal drift velocity of the particle, resulting in a decreased total poloidal drift velocity. Unlike the  $E_r = 0$  case, this particle is not lost but remains well confined near the magnetic axis. Under  $E_r = +10$  kV/m, the deeply helically trapped particles rapidly drift poloidally in the  $\theta = 2\pi$  direction and then drift outward when crossing the out midplane. The particle is confined temporally at the flux surface near the plasma edge but is eventually lost. In this case, the direction of the additional poloidal drift velocity induced by  $E_r$  aligns with the inherent poloidal drift velocity of the particle, leading to a significantly enhanced total drift velocity in poloidal direction.

## 5. Conclusion

In W7-X, the  $\Delta N/N$  as a function of particles initial position in the  $\theta - \zeta$  plane shows that the loss region is mainly in the minimum  $|B|$  region and extends along the magnetic field line in the  $\theta - \zeta$  plane. The deeply helically particles with the largest  $\lambda$  is

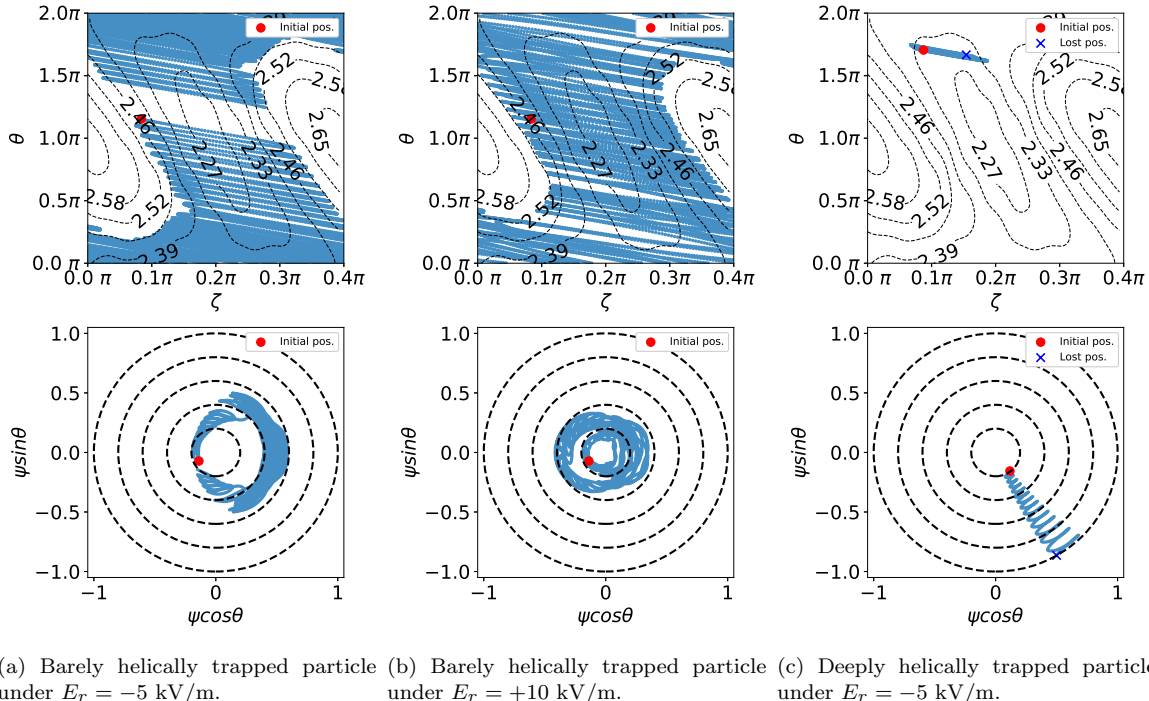


Figure 10: The guiding center orbits of (a) the barely helically trapped particles under  $E_r = -5 \text{ kV/m}$  with  $\lambda = 0.964$  and  $E = 50.9 \text{ keV}$ , (b) the barely helically trapped particles under  $E_r = +10 \text{ kV/m}$  with  $\lambda = 0.964$  and  $E = 50.9 \text{ keV}$ , and (c) the deeply helically trapped particles under  $E_r = -5 \text{ kV/m}$ , lost at  $18.00 C_s/R_0$ , with  $\lambda = 1.033$  and  $E = 50.3 \text{ keV}$  on a flux surface (upper panels) and on a poloidal plane (lower panels).

the dominant loss channel. For the particles initially located at the flux surface close to the magnetic axis (i.e., at the flux surface  $\psi/\psi_w = 0.2$ ), the particles with  $\lambda = [1.000, 1.035]$  exhibit better confinement compared to particles with other  $\lambda$ , indicating the presence of a  $\lambda$  gap for the lost particles in the  $E - \lambda$  phase space. The barely helically trapped particles with  $\lambda = [0.9, 1.0]$  is the second dominant loss channel. This  $\lambda$  gap for the lost particles in the  $E - \lambda$  phase space gradually disappears with increasing  $\psi/\psi_w$ , primarily due to the increasing roughness of the  $|B|$  contours and their greater deviation from the ideal quasi-isodynamic (QI) configuration.

Due to the additional poloidal rotation, under  $E_r = -5 \text{ kV/m}$  and  $E_r = +10 \text{ kV/m}$ , toroidally trapped particles maintain excellent confinement properties and barely helically trapped particles achieve even better confinement. Under  $E_r = -5 \text{ kV/m}$ , the deeply helically particles that are lost are no longer initially located in the minimum  $|B|$  region in the  $\theta - \zeta$  as observed in the 'No  $E_r$ ' case, but instead are found near the outer midplane due to the additional rotation. Under  $E_r = +10 \text{ kV/m}$ , the barely helically trapped particles are almost entirely confined due to the additional rotation, making the deeply helically trapped particles the only lost particle type. These particles are most likely to lose confinement when crossing the outer midplane, after which they become temporarily trapped near the flux surface at the plasma edge before being lost due to their larger orbit width.

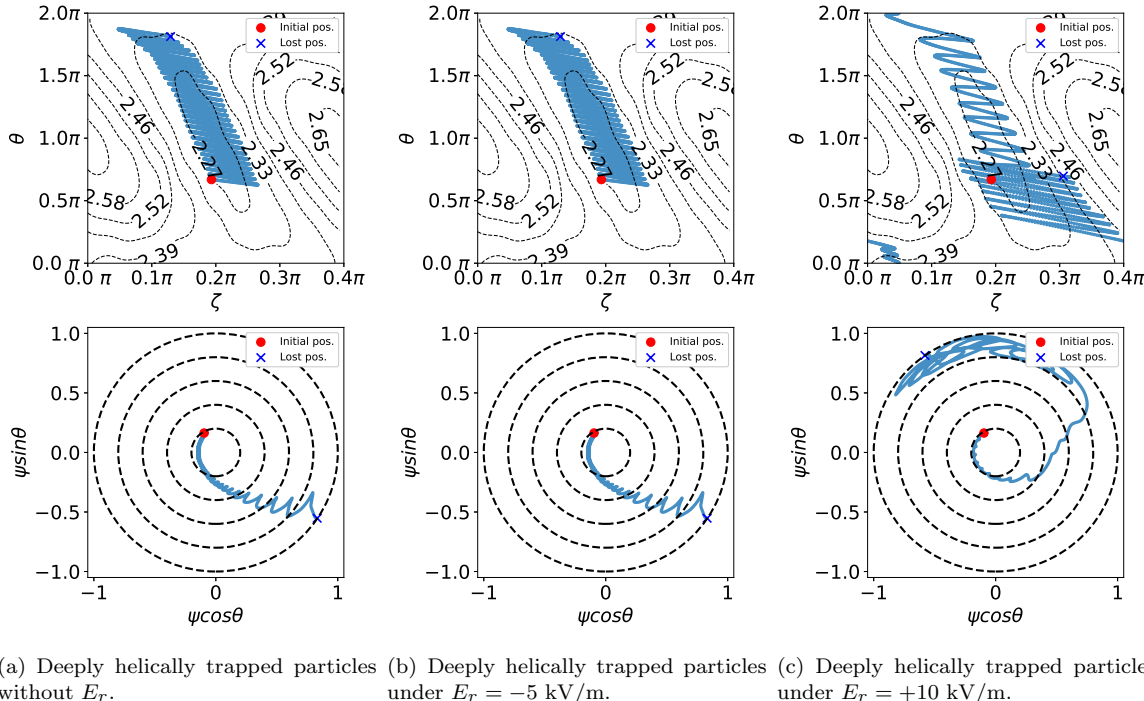


Figure 11: Comparison of guiding center orbits for the same deeply helically trapped particle, initially located near the minimum  $|B|$  contours with  $\lambda = 1.051$  and  $E = 53.2$  keV, under three different radial electric field conditions:  $E_r = 0$  (panel a, lost at  $36.67 C_s/R_0$ ),  $E_r = -5$  kV/m (panel b), and  $E_r = +10$  kV/m (panel c, lost at  $26.90 C_s/R_0$ ). The trajectories are shown both on a flux surface (upper panels) and on a poloidal plane (lower panels).

## References

- [1] P Helander, C D Beidler, T M Bird, M Drevlak, Y Feng, R Hatzky, F Jenko, R Kleiber, J H E Proll, Yu Turkin, and P Xanthopoulos. Stellarator and tokamak plasmas: a comparison. *Plasma Physics and Controlled Fusion*, 54(12):124009, nov 2012.
- [2] G Grieger, W Lotz, P Merkel, J Nührenberg, J Sapper, E Strumberger, H Wobig, R Burhenn, V Erckmann, U Gasparino, L Giannone, H J Hartfuss, R Jaenicke, G Kühner, H Ringler, A Weller, F Wagner, the W7-X Team, and the W7-AS Team. Physics optimization of stellarators. *Physics of Fluids B: Plasma Physics*, 4(7):2081–2091, 07 1992.
- [3] J Geiger, C D Beidler, Y Feng, H Maaßberg, N B Marushchenko, and Y Turkin. Physics in the magnetic configuration space of w7-x. *Plasma Physics and Controlled Fusion*, 57(1):014004, nov 2014.
- [4] Norbert Rust, Bernd Heinemann, Boris Mendelevitch, Alan Peacock, and Michael Smirnow. W7-x neutral-beam-injection: Selection of the nbi source positions for experiment start-up. *Fusion Engineering and Design*, 86(6):728–731, 2011. Proceedings of the 26th Symposium of Fusion Technology (SOFT-26).
- [5] K. C. Shaing and E. C. Crume. Bifurcation theory of poloidal rotation in tokamaks: A model for l-h transition. *Phys. Rev. Lett.*, 63:2369–2372, Nov 1989.
- [6] S. Taimourzadeh, L. Shi, Z. Lin, R. Nazikian, I. Holod, and D. Spong. Effects of rmp-induced changes of radial electric fields on microturbulence in diii-d pedestal top. *Nuclear Fusion*, 59(4):046005, feb 2019.
- [7] J. Y. Fu, J. H. Nicolau, P. F. Liu, X. S. Wei, Y. Xiao, and Z. Lin. Global gyrokinetic simulation of neoclassical ambipolar electric field and its effects on microturbulence in W7-X stellarator.

*Physics of Plasmas*, 28(6):062309, 06 2021.

- [8] W H Wang, J Bao, X S Wei, Z Lin, G J Choi, S Detrick, A Kuley, C Lau, P F Liu, and T Tajima. Effects of equilibrium radial electric field on ion temperature gradient instability in the scrape-off layer of a field-reversed configuration. *Plasma Physics and Controlled Fusion*, 63(6):065001, apr 2021.
- [9] Y C Chen, Y Q Qin, G Y Sun, and Z Lin. The performance of equilibrium radial electric field shear on microturbulence with different magnetic shears in tokamak plasmas. *Plasma Physics and Controlled Fusion*, 65(7):075005, may 2023.
- [10] Katsumi Ida. Experimental studies of the physical mechanism determining the radial electric field and its radial structure in a toroidal plasma. *Plasma Physics and Controlled Fusion*, 40(8):1429, aug 1998.
- [11] S. Äkäslompolo, M. Drevlak, Y. Turkin, S. Bozhenkov, T. Jesche, J. Kontula, T. Kurki-Suonio, R.C. Wolf, and the W7-X Team. Modelling of nbi ion wall loads in the w7-x stellarator. *Nuclear Fusion*, 58(8):082010, jun 2018.
- [12] N. Pablant, A. Langenberg, A. Alonso, J. Baldzuhn, C.D. Beidler, S. Bozhenkov, R. Burhenn, K.J. Brunner, A. Dinklage, G. Fuchert, O. Ford, D.A. Gates, J. Geiger, M. Hirsch, U. Höfel, Ye.O. Kazakov, J. Knauer, M. Krychowiak, H. Laqua, M. Landreman, S. Lazerson, H. Maaßberg, O. Marchuck, A. Mollen, E. Pasch, A. Pavone, S. Satake, T. Schröder, H.M. Smith, J. Svensson, P. Traverso, Y. Turkin, J.L. Velasco, A. von Stechow, F. Warmer, G. Weir, R.C. Wolf, D. Zhang, and the W7-X Team. Investigation of the neoclassical ambipolar electric field in ion-root plasmas on w7-x. *Nuclear Fusion*, 60(3):036021, feb 2020.
- [13] J.M. Faustin, W.A. Cooper, J.P. Graves, D. Pfefferlé, and J. Geiger. Fast particle loss channels in wendelstein 7-x. *Nuclear Fusion*, 56(9):092006, jul 2016.
- [14] J Riemann, R Kleiber, and M Borchardt. Effects of radial electric fields on linear itg instabilities in w7-x and lhd. *Plasma Physics and Controlled Fusion*, 58(7):074001, may 2016.
- [15] Allen H. Boozer. Plasma equilibrium with rational magnetic surfaces. *The Physics of Fluids*, 24(11):1999–2003, 11 1981.